Experimental Study of Upward Flame Spread and Burning of an Inclined Fuel Surface

M.J. Gollner[a,*], X. Huang[a], J. Cobian[a], A.S. Rangwala[b], F.A. Williams[a]

[a] *University of California, San Diego, Department of Mechanical and Aerospace Engineering, 9500 Gilman Drive, La Jolla, CA 92093-0411, United States*
[b] *Worcester Polytechnic Institute, Department of Fire Protection Engineering, 100 Institute Road, Worcester, MA 01609-2280, United States*

Keywords: Flame spread, Inclined Fuel, PMMA, Burning Rate

Corresponding Author: Michael J. Gollner
University of California, San Diego
9500 Gilman Dr.
La Jolla, CA, 92093-0411
U.S.A.
Phone: (858)534-6123
Fax: (858)534-5354
Email: mgollner@ucsd.edu

Preferred Colloquium: Fire Research

Paper length: **6121 words** (79 words available, *Method 1*)
Text = 4716 words (Word Processor)
Equations = 0
Nomenclature = 0
References = $(19 + 2) \times 2.3 \times 7.6 = 367$ words
Tables = 0
Figures = $6 \times (285 + 10) \times 2.2 \times$ 1col.
+ words in captions 280 = 1033 words

Abstract length: 156 words (144 words available)

Color Reproduction: Not Required

*Corresponding author
Email address: mgollner@ucsd.edu (M.J. Gollner)

Abstract

A thermally thick slab of polymethyl methacrylate was used to study the effects of the inclination angle of a fuel surface on upward flame spread. While investigation of upward spread over solid fuels has typically been restricted to an upright orientation, inclination of the fuel surface from the vertical is a common occurrence that has not yet been adequately addressed. By performing experiments on 10 cm wide by 20 cm tall fuel samples it was found that the maximum flame-spread rate, occurring nearly in a vertical configuration, does not correspond to the maximum fuel mass-loss rate, which occurs closer to a horizontal configuration. A detailed study of both flame spread and steady burning at different angles of inclination revealed the influence of buoyancy-induced flows in modifying heat-flux profiles ahead of the flame front, which control flame spread, and in affecting the heat flux to the burning surface of the fuel, which controls fuel mass-loss rates.

1. Introduction

Evaluation of the fire hazard of a material often entails estimation of the material's flame-spread and heat-release rates at full scale by means of interpretation of reduced-scale tests. Maxima of these quantities are important in determining the worst-case scenario used in design of a fire-detection or suppression system [1]. In this study, the flame-spread rate and fuel mass-loss rate (proportional to the heat-release rate) were found to reach maximum values at different orientation angles, implying that the "worst-case scenario" may depend on the orientation selected for evaluation.

This study will seek to explore what controls the mass-loss rate and spread rate by investigating the spatial heat-flux profile ahead of the burning surface, the local regression of the fuel surface and the flame standoff distance over the fuel surface for upward spread and steady burning of surfaces with different orientations. For this investigation, the steady and spreading experiments are performed on polymethyl methacrylate (PMMA). Buoyancy is known to have a significant effect on the flame length, ignition and extinction limits, all of extreme importance for fire prevention and control [2], and the effect of buoyancy varies with orientation. As the lengths of samples increase, the transition from laminar to turbulent flow behavior also plays a role. The results of this study have implications concerning designs for fire safety and may help to increase understanding of flame spread at inclinations found above or below rooftops and in wildland fire spread up sloped terrain.

2. Related Literature

While there have been many studies of upward flame spread along vertical surfaces and of horizontal flame spread along horizontal surfaces, few investigations have systematically addressed the dependence of the spread rate on the orientation angle of the surface for inclined surfaces. To date, with few exceptions all such experimental studies have focused on PMMA as a model fuel, but even for this fuel, the entire range of upward-spread inclination angles

has not yet been addressed. Ito and Kashiwagi [3] report careful, detailed measurement mainly of downward flame spread along PMMA surfaces of different orientation angles, although they do include three somewhat upward orientations. Drysdale and Macmillan [4] were the first to perform upward-spread experiments systematically at different orientations. They studied both thermally thin computer cards and thermally thick PMMA samples 2–6 cm wide. Starting from horizontal spread, they found little change in the average spread rate until the angle, 90° for horizontal, became about 75°, after which the spread rate increased substantially as the orientation of the surface approached the vertical, 0°, but they did not go beyond the vertical to investigate upward spread with flames below the fuel surface, orientations that are investigated here. Pizzo et al. [5] and Xie and DesJardin [6] also investigated flame spread over the surface of PMMA in the same range, 0° to 90°, the former performing experiments on thick samples 20 cm wide, and both making 2-D numerical simulations; the latter also provide additional numerical details of the average gas-phase heat-transfer process during spread. For thermally-thin fuels, Quintiere [7] developed a flame-spread theory using a modified Grashof number to account for gravity along with heat-transfer correlations from Ahmad and Faeth [8] and from Roper et al. [9]; experimental results were in qualitative agreement with predictions.

Steady burning experiments relevant to the present study have been performed by Ohtani et al. [10], who used square sheets of PMMA 3–10 cm wide and found maximum burning rates in the vertical configuration, reaching minima at the pool and ceiling configurations. Much earlier, Blackshear and Kanury [11], who used fuel-soaked wicks 10.54 cm square, also found minimum rates for the horizontal orientation and maxima for vertical orientations, consistent with these results and in qualitative agreement with more recent detailed numerical simulations by Ali et al. [12], but within experimental accuracy they report negligible differences between the vertical and ceiling orientations. Contrary to all other results, de Ris and Orloff [13], who used a gas burner 0.65 m in length, the orientation of which could be varied by rotating it, found that

turbulent burning rates reached a maximum near the pool-fire configuration and minimum near the ceiling-fire configuration. They attribute their conflict with the pervious experiments, which were conducted at smaller scales, of widths less than 10 cm, to various influences, especially radiation and transition to turbulence. The differing previous results for steady burning raise questions about what should be expected in the present experiments.

3. Experimental Setup

An experimental apparatus was constructed that enables measurements to be made of flame spread and mass-loss rates on an inclined fuel surface. Two 30 cm high aluminum angle bars were mounted vertically on a load cell and connected to a rotatable aluminum sheet. This served as the test surface and measured 20 cm in width and 65 cm in height. A sheet of SuperWool insulating board, 1.27 cm thick, was attached atop the aluminum sheet. A section beginning 5 cm from the base of the surface of the insulating sheet was cut out for the fuel sample, a 1.27 cm thick, 10 cm wide, 20 cm tall sheet of Acrylite GP (PMMA), which was then mounted to the aluminum sheet with four screws. Spacers were installed in the back of the sample to align the sample flush with the insulation and to minimize heat losses to the aluminum sheet. To permit unobstructed natural convection, which may occur in practical situations, no side walls were attached.

PMMA samples were cut precisely using a LaserCAMM, including 4 mounting holes and holes for 7 surface-mounted thermocouples. K-type thermocouples, of 0.25 mm diameter wire, were threaded through holes in the sample, bent atop the surface, and then melted flush onto the face of the surface with a heated piece of metal. Thermocouple wires were passed through a 5 cm wide opening along the length of the aluminum sheet, and their outputs were recorded at 10 Hz by a data acquisition system. This opening also facilitated observation of bubbling through the rear of the sample.

Heat fluxes were measured with an array of thin-skin calorimeters, 11 mounted along the

centerline of the sample. Each sensor consisted of a 1 cm square, 1.2 mm thick 304 stainless steel plate painted matte black on the front surface, with a K-type thermocouple spot-welded to the rear of the surface. Heat fluxes were determined by numerically differentiating the measured temperature change of the rear of the sample, taking into account convective, radiative, and conductive losses [14]. Three cameras were placed around the sample to view the flame height, the flame standoff distance, and bubbling, through the front, side, and rear of the sample, respectively. The load cell measured the mass of the sample at 15 Hz with an accuracy of ± 0.5 g.

Ignition of samples undergoing upward flame spread was achieved by igniting a fuel-soaked wick at the base of the sample. The fuel chosen was methyl decanoate, of which 3 mL was used. All samples were ignited at 60° from the vertical, where the wick was left to burn for 2 minutes before a cover made of SuperWool insulating board was removed from the top 18 cm of the sample and the setup was rotated to the desired angle of inclination. In this manner, all samples experienced the same extent of external heat input during the ignition stage, and all had approximately a 2 cm PMMA pyrolysis height at the beginning of the experiment. Steady burning samples were ignited by a standard blowtorch, which was passed over the surface for approximately 2 minutes until the entire surface was uniformly ignited. Measurements on steadily burning samples were taken once a constant rate of mass loss was reached, about 2 to 4 minutes after removal of the insulating board. Between four and nine tests were performed at each inclination in order to test the repeatability of the experimental results.

4. Measured Flame-Spread and Mass-loss Rate

The spread rate, V_p was defined as the rate of increase of the pyrolysis height, which was determined from the readings of the surface-mounted thermocouples under the assumption that the pyrolysis temperature is $T_p = 300°\mathrm{C}$, based upon comparison of the rear-view observations of bubbling and previous measurements on Acrylite [15]. While upward flame spread is typically

acceleratory, the change in spread rate over the relatively small distances measured is not great, and for consistency in comparison with previous experiments [3–6], an average spread rate between distances of 10 cm and 20 cm is employed here. Linear fits were applied to the averaged pyrolysis height to determine representative spread rates from their slopes. The points are averages for all tests and the error bars show the maximum variations between evaluating rates at 10 cm and at 20 cm for all tests. The results are shown in Fig. 1 for $-60^\circ \leq \theta \leq 60^\circ$, along with earlier results from the literature cited previously [3–6]. Despite the evident scatter, to be expected because of the different sizes and distances studied, there is reasonable agreement with the previous work over the common range of angles measured, but the present work shows that the maximum of the curve occurs not exactly at the vertical orientation but rather at somewhat negative angles, as if a symmetrical curve were shifted slightly to the left. These new observations of V_p in the range $-60^\circ \leq \theta \leq 0^\circ$, on the undersides of materials indicate that spread rates at -30° and -45° in fact very closely match the spread rates observed in the 0° configuration, with -30° spread rates slightly higher than the averaged 0° rate.

[Figure 1 about here.]

The mass-loss rates per unit area, obtained in the present study and in two previous investigations, are shown in Fig. 2. The "steady" rates reported here are averages, measured 800–1000 s after the uniform ignition of the entire sample, selected because the measured mass-loss rate was most constant during this period, even though the measured PMMA back-face temperature reached values as high as 80°C by the end of the measurement. For the spreading tests the measured mass-loss rates and pyrolyzing surface areas increase with time, and the results shown in the figure are average values at the time that the pyrolysis front reaches the top of the sample, the total sample area being employed to evaluate the rate per unit area. As may be expected, these rates are significantly less than the "steady" rates, which are higher because of the higher average PMMA temperature associated with the deeper penetration of the thermal wave into

the material at the later time [16]; at about 250 s after the "spreading" measurements shown, the recorded mass-loss rates are comparable with those of the "steady" measurements. The principal observation to be made from these results is that both sets of data exhibit the same dependence on inclination angle, with rates increasing continuously from ceiling through vertical to pool configurations. The "steady" data thus serve to demonstrate that the "spreading" results are not artifacts of the spread process but instead reflect quite general influences of the inclination angle for these experimental conditions. If results during spread had been compared at the same time after ignition instead of at the same extent of fuel involvement, there would be a tendency for the nearly constant slope of the curves to decrease with increasing angle, but the general trend would be the same.

[Figure 2 about here.]

It is noteworthy that, between the vertical and pool configurations, these results are qualitatively different from those of Ohtani et al. [10], obtained with the same fuel, shown in the figure. Those results, which pertain to steady burning of appreciably smaller samples and agree qualitatively with experiments of Blackshear and Kanury [11], are what one would expect for convection-controlled burning, because the component of gravity parallel to the fuel surface is maximum in the vertical configuration. Also, since convection-controlled rates would increase with decreasing boundary-layer thicknesses, the observed higher average mass-loss rates per unit area for the smaller samples are expected for this mechanism; in fact, data in that paper point toward a decrease in the rate per unit area with increasing size. It thus appears that in the present experiments, at least between the vertical and pool configurations, the controlling mechanism is different from that of the smaller samples.

On the other hand, the observed dependence on angle is seen in Fig. 2 to be similar to that of de Ris and Orloff [13] over the entire range. They used a gas burner to simulate flame spread over a large fuel surface up to 65 cm in length, employing a novel technique to identify the

dependence of burning rates on B numbers from measurements of the heat flux to the surface. A fuel mass-transfer number of $B = 1$, similar to the fuel in this present study ($B = 1.67$ [17]) is selected here from de Ris and Orloff to show for comparison. Our mass-loss rate per unit area in both steady and spreading tests over PMMA have nearly the same slopes with θ as the steady gas burner experiments, consistent with the mechanism occurring being the same. This increase in $\dot{m}''$ with θ was attributed by de Ris and Orloff to adjustments involving the importance of radiant fluxes in controlling the rates, thereby suggesting that radiant transfer is important in the present experiments. The scale of the test sample here, however, is significantly smaller than the gas-burner's dimensions, consistent with the lower rates found here, if radiation is controlling and the radiating volume is less, but perhaps surprising in view of the magnitude of the size difference. It may suggest a greater propensity for radiant emissions from PMMA than from typical gaseous fuels.

5. Radiant-Flux Estimates

Because of these mass-loss findings, additional heat-flux measurements were made for the purpose of estimating radiant energy fluxes to steadily burning surfaces. The absence of instrumentation for direct measurement necessitated employing a roundabout, inaccurate procedure. First, heat-flux gauges were placed at various locations well outside the fire and oriented to see the entire flame, in order to obtain the total radiant power output from estimated view factors based on observed flame sizes and shapes. Next, view factors between the burning surface and the flame were estimated for each case and then employed, under the assumption of isotropic emission, to calculate the incident radiant flux. In most cases, resulting heat fluxes from different gauges based on different assumptions differed by less than a factor of two, but with the flames on the underside, at the most negative angle, visual access of the gauges without excessive heating or reflection from surfaces was difficult to achieve, and uncertainties approached a factor of 10. Nevertheless, the order of magnitudes of the resulting fluxes were comparable with the total

fluxes measured on the wall just above the burning surface and calculated as required for gasification from the measured mass-loss rate[1]. It thus was estimated that the radiant contribution varied from about 10 percent to about 70 percent. Moreover, a definite increase in the radiant flux with increasing angle of inclination of the surface was calculated from these results, as seen in Fig. 3. It should be emphasized that the curve shown for the radiant flux, which lies within all error bars, is merely an estimate based on our understanding of the situation and is not a least-squares or polynomial fit, which would not be meaningful because of the wide scatter.

[Figure 3 about here.]

It is understandable, for a number of reasons, that radiant fluxes will increase with angle. The flux is mainly from soot emissions, the intensity of which will increase with increasing soot volumes and concentrations, and the soot is produced by finite-rate processes in fuel-rich zones, so that longer fuel-rich residence times lead to more soot and greater emissions. That residence time will be minimum with the flames, largely blue, underneath the fuel surface and maximum with the flames rising above, in the pool-burning configuration. In addition, the pool-burning view angle between the flames and the burning surface is greatest, most of the yellow flames at the negative angles being adjacent to or behind inert walls. Coupled with the much thinner flame zones at negative angles, a monotonic increase of the radiant contribution with increasing angle is clearly to be expected. The increase in the rate of radiant energy transfer therefore is consistent with the burning-rate increase seen in Fig. 2 and a viable candidate for its cause.

6. Measurement of Flame-Standoff Distances

The three-dimensional character of the flow complicates efforts to measure flame-standoff distances photographically. The side-view camera is most useful for this purpose, but it mainly

[1]Total heat fluxes over the fuel surface are estimated via an energy balance, $\dot{q}''_p = \dot{q}''_{rr} + \dot{m}''\Delta H_p$, where $\dot{q}''_{rr} \approx \sigma T_p^4 = 6.1$ kW/m^2 is the re-radiation to the fuel surface, assuming the surface temperature to be equal to T_p and the surface emissivity equal to 1, $\dot{m}''$ is the steady mass-loss rate per unit area measured in Fig. 2 and $\Delta H_p = 1,620$ kJ/kg the effective heat of gasification [18, 19]

senses the maximum distance, normal to the fuel surface, of emission of flame radiation, in the horizontal line of sight parallel to the surface. The horizontal variations are small between ceiling and vertical configurations, but they rapidly become large as the pool configuration is approached. Also, while some blue flames are visible near the leading edge in ceiling-like configurations, most of the flames detected are yellow. The flame characteristic that can be detected most accurately is the outer boundary of the yellow zone (or, sometimes near the leading edge, where there is no yellow, the blue zone), and for this reason that is what is recorded here. For present purposes, the "flame standoff" distance is therefore defined as the distance between the top of the yellow flame and the fuel surface, perpendicular to the fuel surface, measured by side-view images of the flame. This is more nearly a measurement of the maximum soot-emission height of the flame for orientation angles from 30° to 60°, but much more representative of maximum-temperature positions for $-60° \leq \theta \leq 0°$. The distances, measured by a custom thresholding script in MATLAB on images taken during a "steady" burning regime, averaging over approximately 50 images from several tests at each angle corrected for regression of the fuel surface, are plotted in Fig. 4. Similar results are observed for "spreading" tests, as expected, but they vary a little more and could complicate interpretations because of the spreading nature of the flame.

The "standoff distance" in Fig. 4 remains similar for ceiling and vertical configurations and begins to linearly lift off the surface as pool configurations are approached. Underside measurements of y_f can be interpreted from considerations of boundary layers in natural convection. In such flows, in general, it can be reasoned that it is the component of gravity parallel to the fuel surface that accelerates the flow, the normal component merely adjusting the normal pressure variation, and by dimensional analysis, characteristic lengths should then be proportional to the cube root of the ratio of the square of the kinematic viscosity to this component, which would vary inversely as the cube root of $\cos\theta$. It may then be inferred that the standoff distance should

approximately exhibit such a variation, although the classical laminar boundary-layer theory for a vertical wall produces a fourth-root dependence, instead, the additional dimension modifying this simple dimensional reasoning in the boundary-layer approximation. While results also differ for turbulent boundary layers, a roughly fractional-power dependence in general is to be expected.

Comparison of the curves for the "wall fire" and negative angles in Fig. 4 exhibit consistency with this deduction, within experimental accuracy, near the leading edge, where the flow is most nearly two-dimensional. The experimental accuracy is insufficient to determine the power, but a fractional power clearly is indicated near the leading edge. Farther along the burning surface, however, this relationship reverses, and the "wall fire" exhibits a larger standoff distance. This is consistent with the flow remaining nearly two-dimensional for the vertical configuration but becoming increasingly three-dimensional as the ceiling configuration is approached, with fluid outflow to the sides, as may be seen in the left-hand photograph in Fig. 3, leading to a reduction in the standoff distance, which is seen to actually begin to decrease with increasing distance from the leading edge at large distances, through these three-dimensional outflow effects.

Because of this effect, the average rate of convective heat transfer to the burning fuel may decrease with increasing angle, in which case the increased radiative heat transfer rate must necessarily become responsible for the increase of the burning rate. A consequence of these observations is that standoff distances (but not burning rates) would behave differently for wider samples that maintained more nearly two-dimensional flow.

The sharp increase in the measured y_f for positive θ occurs through what could qualitatively be called "liftoff" of the flame from the fuel surface by vertical buoyant acceleration. Within this region of linear increase of the "standoff distance" with distance from the leading edge, a flame liftoff angle, ϕ can be measured as the angle between y_f and the fuel surface. For "steady" tests, ϕ is measured to be 32°, 18°, 10° and 8° for inclinations of 60°, 45°, 30° and 0°, respectively;

a rapidly accelerating increase in ϕ with θ. The increase of the component of gravitational acceleration perpendicular the fuel surface causes this increase, as well as the inward "necking" of the flame, seen in the other photograph in Fig. 3. These "standoff distances" thus are seen to be very three-dimensional phenomena and to represent mainly the behavior near the center of the fuel for angles above 30°.

[Figure 4 about here.]

The air entrainment from the sides causes the "necking" of the flame above the fuel sample, pushing flames at the edges of the sample closer to the fuel surface and extending y_f above the center of the fuel. This three-dimensional behavior is the cause of the result in Fig. 3, where constriction of the center of the 60° flame is caused by increased air entrainment at the edges of the sample, an effect previously observed by Ito and Kashiwagi [3]. At underside and vertical orientations the flame shape remains fairly uniform over the fuel surface except for slight effects at the edges of the sample, but as the fuel is inclined between 30° and 60° three-dimensional lifting becomes increasingly important.

[Figure 5 about here.]

Width effects on a vertical fuel sample have been studied by Rangwala et al. [20] and Tsai [21] previously, and in their experimental results only small changes appear to take place between widths of 10 to 20 cm. When the fuel is inclined, however, these changes may become more significant. To investigate this, regression measurements were made transversely on quenched samples. The results are shown in Fig. 5, where the measured regression of the sample surface has been used to deduce the variation in the mass-loss rate across the sample width. Samples were cut along the width at 10 cm above the leading edge and photographed along with a scale, measuring the fuel thickness manually from photographs with ImageJ. The mass-loss rate per unit area was found from the regression length, r by $\dot{m}'' = r\rho_s/t_b$, where $\rho_s = 1190$ kg/m^3 is the density of PMMA [19] and t_b the burning time of the sample.

While for the $-60°$ and $0°$ tests the regression is fairly uniform across the width of the sample, significantly higher variations in the mass-loss rates per unit area are found across the width of the sample in the $60°$ orientation. Small edge effects are present in all samples as a result of a lip that forms between the fuel surface and insulation as the surface regresses with time. Linteris et al. found similar effects on horizontal PMMA samples when compared to vertical samples burned under imposed heat fluxes on the cone calorimeter [22]. The principal result of the present measurements, however, is the large increase in the local burning rates at the edges in pool-like configurations, resulting from greatly increased convective heat transfer there by the flow drawn into the fire plume, despite the likely dominance of radiative transfer in affecting the total mass burning rate at these orientations. The edge convective enhancement adds to the nearly uniform radiant contribution.

7. Heat-Flux Distributions

To complete the experimental information used in interpreting the spread-rate results of Fig. 1, heat-flux distributions were obtained from the array of gauges on the wall above the samples. While the results clearly vary with time, complete profiles above the burning fuel are obtainable only when the pyrolysis front reaches the top of the sample. Since the general character of the results is not likely to be very different over the 10 cm to 20 cm distance of interest, results are reported only for the time at which the pyrolysis front reaches the top. Heat-transfer correlations of the transition length along an inclined, heated surface [23] may suggest that the flow in this experiment is mostly laminar along its length, but correlations for the convective heat flux to the fuel surface are not reliable because of large effects of differences in configurations, which change resulting correlations drastically. These effects may be similar to the "necking" and liftoff behavior which is dependent on the width and would be affected by sidewalls. The flux $\dot{q}''_f(x)$, which was directly measured in this study for $x = 22.5$ to 47.5 cm above the leading edge of the sample, is shown in Fig. 6.

[Figure 6 about here.]

The axes of the figure are selected so that power-law fits to the decay with height of the heat-flux profiles will appear as straight lines. The horizontal scale thus is logarithmic, like the vertical scale, even though the range of values on the horizontal scale, not much more than a factor of two, is small enough that this may not be evident initially. The dashed lines, showing best power-law fits, exclude the first two data points, nearest to the pyrolysis front, where the flux maintains the nearly constant value presumed to exist in that region of the pyrolyzing surface. It is seen that the power-law decay is quite reasonable in the region of the fit. Other fits were tested, such as exponentials, and were found to be noticeably poorer, although in some cases, especially those in which the fluxes do not change much, it is difficult to determine the best functional dependence clearly.

The power-law fits in Fig. 6 can be expressed as $\dot{q}''_f(x) \sim A(x/x_p)^n$. For $-60^\circ \leq \theta \leq 0^\circ$, the slope of the decay in heat flux is the same, $n \approx -2$, with the constant A decreasing with decreasing θ, although perceptibly larger at -30° than at 0°. In flame spread over the top of inclined fuel surfaces the slope is -5, -6 and -7 for for 30°, 45° and 60°, respectively. While heat fluxes near the fuel surface increase with increasing inclinations (Fig. 3), the net average heat flux to the unignited fuel for positive inclinations is significantly lower than for negative inclinations because of this rapid decay with increasing x.

It is clear that for large angles, radiation controls the burning rate and the view angle to the unignited fuel surface ahead of the burning fuel also decreases with increasing angle. There is also some additional contribution of convective cooling instead of convective heating ahead of the burning fuel surface as the pool-burning orientation is approached. The resulting decreased heat fluxes significantly reduce V_p with increasing θ, explaining the results in Fig. 1 for positive angles. The opposite orientation dependencies of heat fluxes to burning and non-burning fuel is noteworthy at these positive angles. In addition, although three-dimensional flow is clearly

prevalent in the experiments at these angles, the same qualitative differences between heat fluxes to burning and non-burning fuel are to be expected for very wide samples, since the "necking" and enhanced edge regression cause quantitative but not qualitative differences; the general shape in Fig. 1 is not likely to be different for infinite width.

At negative angles, on the other hand, convective heating mainly controls both spread and burning. Despite the increasing outflow to the sides with increasing negative angles, the general behavior of decreasing spread rate and heat flux ahead as the ceiling configuration is approached, seen in Figs. 1 and 6, is also expected in two dimensions, for example from the observed increase of the leading-edge standoff distance. The slightly higher heat flux at $-30°$ compared with $0°$ is consistent with the observed spread-rate maximum in Fig. 1 and indicates a variation notably different from the variation of the heat flux to the burning fuel over that small range of angle. This difference may arise from the mean flow becoming more two-dimensional with increasing distance along the non-pyrolyzing surface; the outflow to the side affects the burning rate but has not yet influenced the heat flux ahead significantly at these angles. The reason for the slight increase of convective heat flux with decreasing angle near vertical is unclear but may be associated with the normal component of gravity pressing the flame closer to the fuel surface, a possibility that deserves further study. In any event, the difference of the maximum from vertical of both the angle and magnitude of the forward heat flux and spread rate are small, so the vertical configuration is useful for studying the most hazardous configuration in this respect. Thus the entire general shape of the curve in Fig. 1 is expected to apply as well for very wide samples.

8. Conclusions

In this work, an experiment was designed to test the effects of surface orientation on burning rates and spread rates. It was concluded that spread rates are greatest in near-vertical orientations while burning rates are maximized in near-horizontal orientations, for the physical reasons

discussed. The experimental design attempted to approach as closely as possible conditions that may be expected to be encountered in practice. In so doing, a number of three-dimensional effects were identified in the experiment. Nevertheless, it was reasoned that the qualitative trends observed, including the spread-rate maximum at angles slightly less than vertical, are general and would also apply in strictly two-dimensional configurations in the size range studied or larger, for both polymeric (and, in some respects, cellulosics, not discussed here) solid fuels like PMMA.

Acknowledgments

The authors would like to thank Alexander Marcacci, Ulrich Neimann and Mario Zuniga for their contributions to laboratory experiments. We are also grateful to the Society of Fire Protection Engineers, Educational and Scientific Foundation for financial resources that enabled this work. Valuable discussions with John de Ris, Jose Torero, Adam Cowlard and Yuji Nakamura are also acknowledged.

References

[1] ASTM E2058-03 - Standard Test Methods for Measurment of Synthetic Polymer Flammability Using a Fire Propagation Apparatus, Technical Report, ASTM International, 2003.

[2] J. L. Torero, L. Bonneau, J. M. Most, P. Joulain, Proc. Combust. Inst. 25 (1994) 1701–1709.

[3] A. Ito, T. Kashiwagi, Combust. Flame 71 (1988) 189–204.

[4] D. Drysdale, A. Macmillan, Fire Safety J. 18 (1992) 245–254.

[5] Y. Pizzo, J. Consalvi, B. Porterie, Combust. Flame 156 (2009) 1856–1859.

[6] W. Xie, P. Desjardin, Combust. Flame 156 (2009) 522–530.

[7] J. Quintiere, Fire Safety J. 36 (2001) 291–312.

[8] T. Ahmad, G. Faeth, Proc. Combust. Inst. 17 (1979) 1149 – 1160.

[9] F. Roper, C. Smith, A. Cunningham, Combust. Flame 29 (1977) 227 – 234.

[10] H. Ohtani, K. Ohta, Y. Uehara, Fire Mater. 18 (1991) 323–193.

[11] P. Blackshear, M. Kanury, Proc. Combust. Inst. 11 (1967) 545–552.

[12] S. Ali, V. Raghavan, A. Rangwala, Combust. Theor. Model. 14 (2010) 495–518.

[13] J. de Ris, L. Orloff, Proc. Combust. Inst. 15 (1975) 175–182.

[14] ASTM E459-05 - Thin Skin Calorimeter, Technical Report, ASTM International, 2005.

[15] K. Saito, J. Quintiere, F. A. Williams, Fire Safety Science 15 (1985) 75–86.

[16] Y. Pizzo, J. Consalvi, P. Querre, M. Coutin, L. Audouin, B. Porterie, J. Torero, Combust. Flame 152 (2008) 451 – 460.

[17] K. Annamalai, M. Sibulkin, Combust. Sci. Technol. 19 (1979) 167–183.

[18] V. B. Apte, R. W. Bilger, A. R. Green, J. G. Quintiere, Combust. Flame 85 (1991) 169–184.

[19] R. Ananth, C. C. Ndubizu, P. Tatem, Combust. Flame 135 (2003) 35–55.

[20] A. Rangwala, S. Buckley, J. Torero, Proc. Combust. Inst. 31 (2007) 2607 – 2615.

[21] K. Tsai, Fire Safety J. 44 (2009) 962–967.

[22] G. Linteris, L. Gewuerz, K. McGrattan, G. Forney, Fire Safety Science 8 (2005) 625–636.

[23] M. Al-Arabi, B. Sakr, International Journal of Heat and Mass Transfer 31 (1988) 559 – 566.

List of Figures

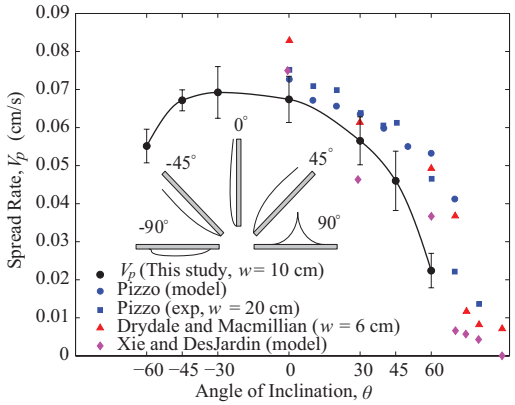

Figure 1: Dependence of the average rate of flame spread V_p on the inclination angle θ of the fuel surface. Here V_p is calculated from thermocouple measurements of x_p the pyrolysis-front position and is compared with previous experimental results by Pizzo et al. [5] and Drysdale and Macmillian [4] and numerical results by Pizzo et al. [5] and Xie and DesJardin [6]. The width of samples tested experimentally, w, is indicated in the figure legend.

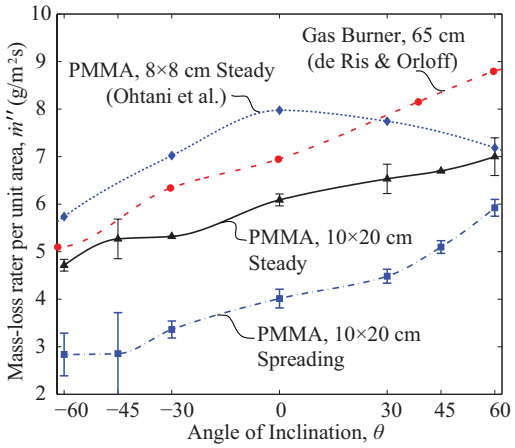

Figure 2: The mass-loss rates per unit area as a function of inclination angle for both steady and spreading tests in this study, along with previous data on 8×8 cm square samples of PMMA by Ohtani et al. [10] and with a 0.65 m long gas burner with $B = 1$ by de Ris and Orloff [13].

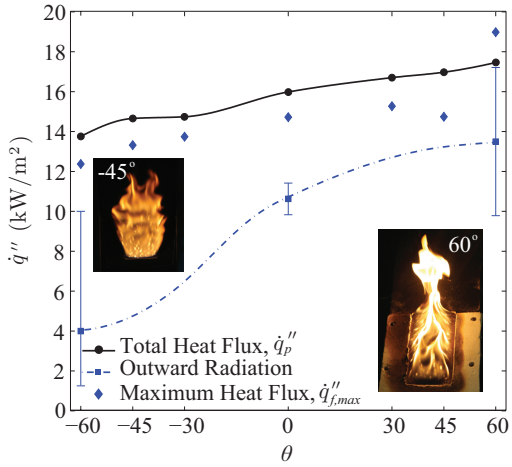

Figure 3: Total heat fluxes over the fuel surface, $\dot{q}_p''$, estimated radiant energy fluxes and maximum measured heat fluxes above the fuel surface, $\dot{q}_{f,max}''$ are presented for steady burning tests. Error bars denote the standard deviation of variations between tests, except for $-60°$ where only the most reasonable results are shown. Inset photographs of $-45°$ and $60°$ tests are also shown.

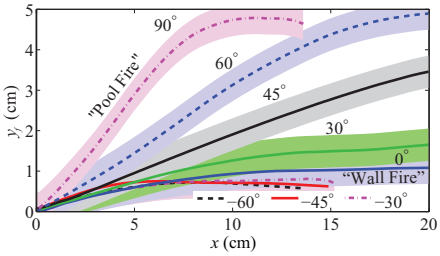

Figure 4: Standoff distances of steady flames when $x_p = 20$ cm taken by a side view camera. The angle of inclination varies from $-60°$ to $90°$.

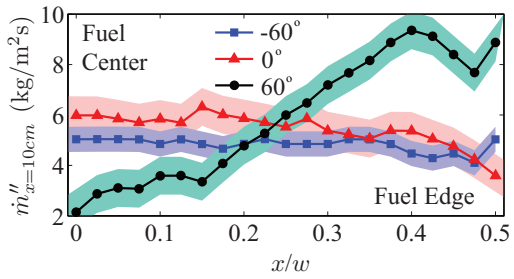

Figure 5: Mass-loss rates from the center to edge of the fuel sample estimated from regression of the surface for steady-burning tests. Shaded regions indicate estimated error bounds.

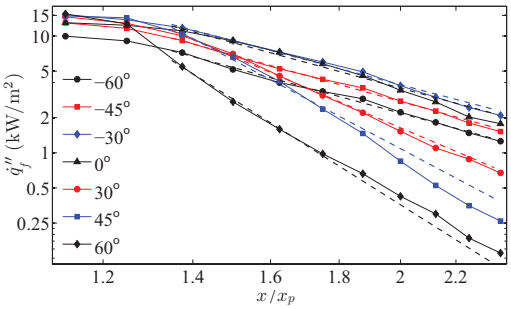

Figure 6: Heat-flux profiles ahead of the spreading fuel sample, where $x_p = 20$ cm.